DISCHARGE INITIATION EXPERIMENTS IN THE TOKAPOLE II TOKAMAK

by

DAVID ADNA SHEPARD

A thesis submitted in partial fulfillment of the

requirements for the degree of

Doctor of Philosophy

(Physics)

at the

UNIVERSITY OF WISCONSIN-MADISON

1984

DISCHARGE INITIATION EXPERIMENTS

IN THE TOKAPOLE II TOKAMAK

David Adna Shepard

(Under the supervision of Associate Professor Stewart C. Prager)

Experiments in the Tokapole II tokamak demonstrate the benefits of high density ($n_e/n_o > 0.01$) preionization by reducing four quantities at startup: necessary toroidal loop voltage (V_1) (50%), volt-second consumption (40-50%), impurity radiation (25-50%), and runaway electron production (~ 80-100%). A zero-dimensional code models the loop voltage reduction dependence on preionization density and predicts a similar result for reactor scale devices. The code shows low initial resistivity and a high resistivity time derivative contribute to loop voltage reduction.

Microwaves at the electron cyclotron resonance (ECR) frequency and plasma gun injection produce high density preionization, which reduces the initial V_1, volt-second consumption, and runaways. The ECR preionization also reduces impurity radiation by shortening the time from voltage

application to current channel formation. This, evidently, reduces the total plasma-wall interaction at startup.

The power balance of the ECR plasma in a toroidal-field-only case was studied. Langmuir probes and impurity doping were used. The vertical electric field (E_v) and current (I_v), which result from curvature drift, were measured ($E_v \sim 10$ V/cm and $I_v \sim 50$ Amps) and exceeded expected values for the bulk electron temperature (~10 eV). Presumably, the electron distribution function is non-Maxwellian, and the E_v and I_v are the result of a population of warm electrons. This is supported by impurity doping, which increases the radiated power while decreasing the warm electron signatures. Apparently, the major power losses are curvature drift and radiation. This implies favorable scaling, in which the required ECR power is linear with scale length (like radius) and not cubic (like volume).

A series of experiments with external windings to simulate field errors perpendicular to the toroidal field was done. The results imply that an error field of 0.1% of the toroidal field is deleterious to ECR plasma density. Such a field error was evidently not present during standard toroidal-field-only operation. A vertical magnetic field was capable of shortening the delay to breakdown, but could not produce the initial loop voltage reduction observed with ECR preionization.

ACKNOWLEDGMENTS

I would like to thank my advisor, Professor Stewart Prager, for his guidance throughout this research and the writing of this thesis. I would also like to thank Professors J.C. Sprott and R.N. Dexter for many helpful suggestions and discussions. In particular I thank Professor Sprott for suggesting this research topic.

The work presented in this thesis could not have been done without the assistance of my fellow graduate students and the support staff directed by T. Lovell with B. Vallem and A. Gordon. In particular, I thank A. W. Leonard who constructed the plasma gun used during a portion of this research. Dr.s R.J. Groebner, A.P. Biddle, D.J. Holly, H.R. Garner, N.S. Brickhouse, T.H. Osborne, D.W. Witherspoon, M. Zarnstroff, and Ms. T. Rempel are thanked for many hours of helpful conversation from the building of Tokapole to the present.

I wish to express my gratitude and appreciation to my parents for their love and patience throughout my student career.

I also thank my wife, Cherie, for her love and encouragement through the good and bad times. And I thank my daughters, Julie and Paula, who were often jealous of the laboratory, but who sometimes demonstrated understanding beyond their years.

Financial support for my research was provided by the U.S. Department of Energy.

TABLE OF CONTENTS

CHAPTER I

Introduction

I. Motivation and Background

Discharge initiation in tokamaks is not as well understood as the steady state equilibrium. The study of gaseous electronics requires extension to toroidal systems with magnetic fields. Linear discharges have been thoroughly studied. For a typical discharge experiment, electrodes form the plasma and drive the discharge current. Usually, there is no magnetic field, and toroidicity is avoided. At startup in a tokamak, plasma formation takes place in the presence of a toroidal magnetic field, without electrodes. This is a transient and rapidly changing phase of tokamak discharges which is not well understood and is difficult to control.

In addition, tokamak studies are driven by the need for a fusion reactor. At present, toroidal systems appear to be the most easily advanced to reactor status. In particular, the tokamak concept may hold the most promise for the first-generation, deuterium-tritium-fueled reactor. The startup

of a tokamak is crucial to the feasibility of an economic reactor. The short pulse (< 24 hrs.) devices require a startup which causes minimal damage and does not lower the efficiency. The proposed, long pulse (> 24 hrs.) devices should not be encumbered with an expensive, over-engineered, startup procedure.

The archetypical tokamak is a pulsed, toroidal, plasma confinement device of circular cross section. A toroidal loop voltage, V_l, breaks down the fill gas. The resultant plasma current, I_p, is inductively driven along the dominant, toroidal, magnetic field, B_t. This current produces a poloidal magnetic field, B_p, which pitches the total field lines into helices. The pitched field lines provide confinement against several loss mechanisms.

Some tokamaks, to which we will refer, are listed in Table 1.1. The relevant device parameters are the major radius, R, the minor radius, a, and the toroidal field, B_t. Plasma parameters of prime concern include I_p, electron density, n_e, and electron temperature, T_e. Typically, these three quantities are measured with an external rogowski coil, a microwave interferometer, and Thompson scattering, respectively.

Excellent reviews[1] explain the physics of tokamaks. The reviews also demonstrate the rise in complexity of the tokamak from its inception to a reactor candidate.

TABLE 1.1

A Representative Group of Tokamaks

Tokamak[2]	a (cm)	R (cm)	B_t (kG)	I_p (kA)	n_e (cm^{-3}) (x 10^{13})	T_e (eV)
ST	13	109	40	70	1.5	2500
PLT	45	130	32	550	8	4000
ISX-B	27	93	12	100	6	1100
JFT-2[3]	25	90	10	70	1.5	~600
Pretext[4]	15	53	<10	60	3	200
Tokapole II[5]	6-10	50	<8	10-40	0.2-1.0	~100

Standard tokamak startup is divided into three parts: breakdown, plasma formation, and current rise [6]. This is shown schematically in Figure 1-1. V_1 is applied to a nearly neutral fill gas at the beginning of the breakdown phase. The departure from neutrality is a few seed electrons ($n_e/n_o \ll 1.0\%$), due to cosmic rays or a preionization source. Most devices need an electron source to assist breakdown.

Breakdown in tokamaks occurs when 1.0 to 10% of the gas is ionized for $T_e \sim 5eV$, and an electron-ion collision is as likely as an electron-neutral collision. Before breakdown is achieved, electron-neutral collisions dominate. This early phase of plasma development is characteristic of unassisted and low density ($n_e/n_o < 1.0\%$) preionization experiments. The term "high density preionization" will imply the achievement of $n_e/n_o > 1.0\%$, before V_1 is applied. The discussion of preionization techniques in Chapter 4 is divided into low and high density regimes.

The current profile is hollow during plasma formation, as a result of the skin effect of the plasma. The current is too low to form a tokamak equilibrium, and the energy confinement time is short. Thus, the plasma temperature is held roughly constant, below 100 eV.

Tokamak equilibrium is achieved during the current rise phase. Ionization of the gas within the hollow profile is nearly

Figure 1-1. Schematic representation of the three phases of startup: 1. Breakdown, 2. Plasma formation, and 3. Current rise.

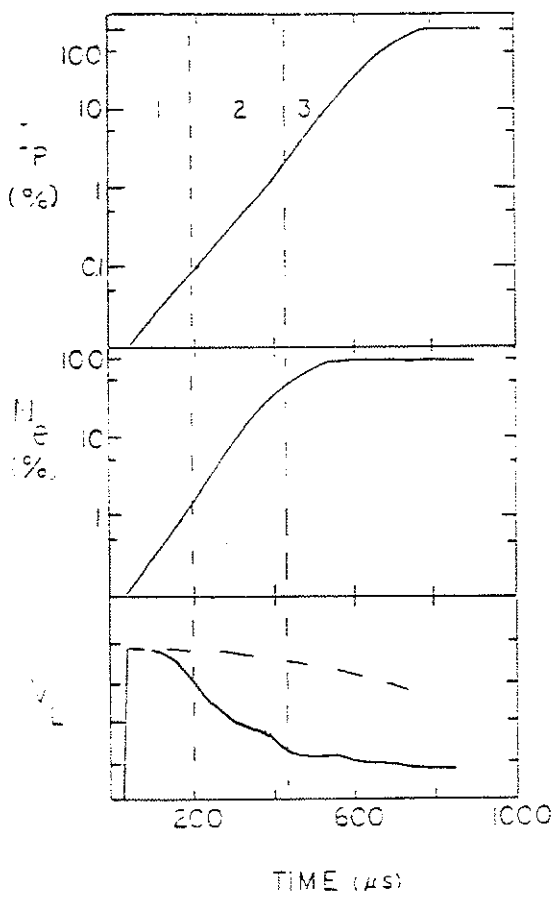

complete. The hollow current profile fills in, and energy confinement improves.

Discharge initiation topics related to gaseous electronics in toroidal magnetic fields include drifts, stray field losses, impurity radiation, and runaway electron production. These topics need to be well understood, so they may be suppressed or controlled. The effect of high density preionization on these quantities needs explanation and experimental verification. Particle drifts in a toroidal field cause severe losses before the current rise phase. Toroidal field errors create another loss channel[4,7] as particles stream parallel to B into the limiter or walls. Low-Z impurities, such as oxygen, radiate and suppress the plasma temperature, until they are "burned through".[8] This occurs when the low-Z impurities are mostly stripped of their electrons and cease to be a major loss channel. Burn-through occurs during current rise and allows temperatures to exceed 100 eV. An artifact of the early, low temperatures is a high resistivity which enhances runaway electron formation. The voltage must be held high to provide ohmic heating during breakdown and current formation, so the tail of the electron distribution function decreases in collisionality and runs away. Besides the health hazard, these runaways can cause significant material damage and impurity reflux.

The mechanisms and parameters of startup need to be understood if a tokamak reactor is to have economic feasibility. The breakdown V_1 scales as the major radius of a tokamak, and reactors may need hundreds of volts for startup, without high density preionization. This implies torus insulation problems, large primary voltages, and runaway electron generation. Also, the consumption of transformer volt-seconds during the non-power-producing, high-voltage startup, is a loss of efficiency.

The pulsed nature of tokamaks is unattractive to power and design engineers and material scientists. A device with the fewest possible startups under the above conditions is needed. A search for a steady state tokamak has led to non-transformer, current drive schemes. These concepts are at present too inefficient for a reactor.[9,10] Thus, an alternative approach has been suggested. A transformer-driven tokamak would be run until saturation. Non-transformer current drive would be applied while the transformer is driven to reverse saturation. This would maintain the plasma current, until the next pulse.

The eventual solution may involve a device with nearly a twenty-four-hour pulse. Such a tokamak would be part of a network which could sustain a regular but brief shutdown. This cycle could ease restrictions on ash removal and daily inspection techniques.

In summary, short-pulse (< 24 hrs.) tokamaks suffer from startup problems listed above. Long-pulse and quasi-steady-state tokamaks have fewer startups and should avoid expensive, complex startup equipment of no use during the equilibrium phase of the discharge.

In tandem with the search for long pulse devices, a different approach is desired. This approach would minimize or eliminate the objections to the startup procedure. To minimize the deleterious effects, the physics of standard startup and possible alternatives must be investigated. Also, the implications for the engineering of such devices must be clarified.

The remedy for most of the above problems proposed by this thesis is high density preionization of the startup gas. The preionization breaks down the gas before the loop voltage is applied. To understand the impact of this, the standard breakdown must be understood. Tokamak breakdown may be discussed in the framework of gaseous electronics. However, the data from gaseous electronics must be considered carefully.

Generally, unmagnetized discharges between flat plate electrodes have been studied at pressures of 0.1 to 10 torr.[11,12] Typically, kilovolts have been applied to plates separated by a few millimeters. Losses are typically governed by diffusion to the walls of the tube. An example would be a sample of gas

between two electrodes separated by a few centimeters. An increasing, from zero, voltage is applied, diffusion losses are ignored, and an ionization source is present to provide primary electrons. The sequence of events is shown schematically in Figure 1-2. At low voltages, the electrons provided by the ionization source are collected and saturation current is drawn. As the voltage increases, the primary electrons gain enough energy to ionize the sample gas. The collected current increases as the newly produced electrons produce more ionizations. This is termed the the Townsend avalanche and combined with the saturation current phase represents the Townsend discharge regime. If the ionization source is removed the discharge is terminated in this regime. At the breakdown voltage, the collected current may increase many orders of magnitude and the discharge becomes self sustaining. This occurs, if the ions produced by one primary electron release at least one secondary electron by impact at the cathode. These impact-released electrons will sustain the discharge if the ionization source is removed. The production of one secondary electron per primary electron is the Townsend criterion for breakdown.

There are major differences in the parameters of linear discharge tubes and tokamaks. Tokamaks utilize one turn voltages between 10 and 100 volts. The path length of an electron is limited by drifts and field errors, and a given electron may make

Figure 1-2. The current-voltage characteristic of a glow discharge experiment, with 1 torr of pressure.

A-B Saturation current plateau

B-C Townsend Avalanche regime

C-D Sub-normal Glow

D-E Normal Glow operation

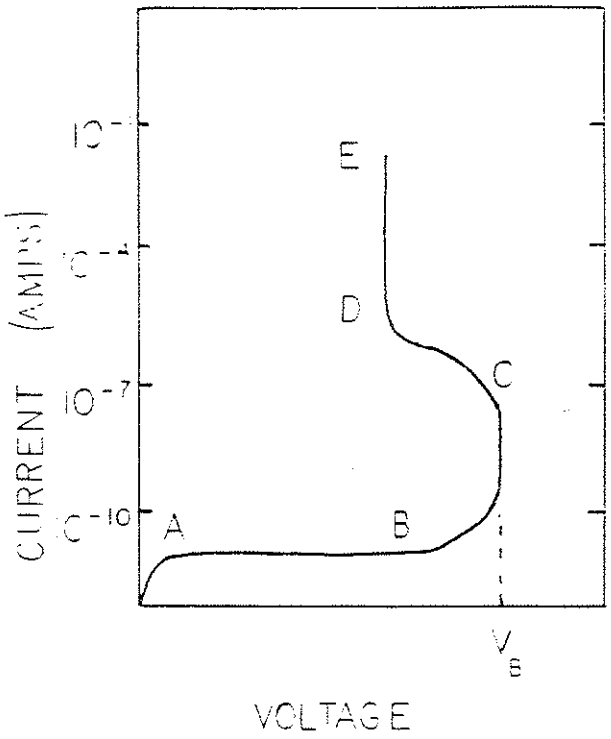

many passes through the volume of gas before being lost to a limiter. Typical fill pressures are on the order of 10^{-4} torr. Despite the disparity of parameters, breakdown in tokamaks is analogous to breakdown in discharge tubes. The loss mechanisms are different, but a Townsend discharge regime must develop before breakdown can occur. The phenomenology of discharge tubes has been adapted to breakdown in toroidal systems by several authors[2,13].

The linear, Extrap, Z-pinch experiment[14] provides an illustration of a system with distances nearer fusion scale lengths, a magnetic field, and voltages on the order of gaseous electronics. A voltage of > 1.0 kV is applied between electrodes 0.2 m apart. No axial magnetic field is applied, but an octupole magnetic field limits the breakdown to a narrow channel along the null and introduces a loss term which modifies the Townsend criterion. Apart from the loss term, the Townsend criterion describes the experiment. A similar loss term may affect the plasma gun preionization experiment, in Chapter Four, and will be discussed there.

The primary source of preionization plasma for this thesis is electron cyclotron resonance (ECR) frequency microwave power. Since tokamaks require auxiliary heating, there has been development of high power microwave sources which make such heating and preionization at the relevant magnetic fields (50 T)

possible. Various incarnations of the gyrotron can provide hundreds of kilowatts for preionization experiments. This raises the issue of the minimum power needed for high density preionization. To determine this, the power balance of a preionization plasma needs to be examined in the framework of a toroidal magnetic field, and gaseous dynamics.

1B. Outline of the Results of This Research

This thesis will describe a wide range of startup experiments done on the Tokapole II tokamak. The primary goal of this research is the understanding and lowering of the following quantities during startup: V_1, volt-second consumption, runaway electron production, and impurity influx. A zero-dimensional code is used to model the effects of a preionization plasma on V_1.

The primary tool to achieve these goals is ECR preionization at microwave frequencies. In addition, Ion Cyclotron Resonance (ICR) frequency power and gun plasma injection are tried as preionization sources.

Studies of the power balance of the ECR preionization plasma are done to reveal and possibly reduce the losses, in order to minimize the ECR power required. In addition, if the losses are

reduced, higher preionization plasma temperatures (T_e > 100 eV) might burn through low-Z impurities before V_1 is applied. Field correction coils, electrostatic biasing of conductors in the plasma, and spectroscopic observations of impurity-doped plasmas are used.

The effects of axisymmetric vertical magnetic fields (B_v) are examined to achieve better particle and energy confinement. A B_v field error coil and a quadrupole B_v for plasma positioning are studied. The ECR plasma density prior to the application of V_1 and the delay to breakdown during V_1 application without preionization are of particular interest.

A description of Tokapole II and the available diagnostics is presented in Chapter 2. Modifications to the device during these experiments are also discussed.

Chapter 3 discusses Tokapole experiments with an ECR plasma, in a purely toroidal field, including results which imply a warm electron component dominates the power balance (50 eV < T_e < 1 keV). The theoretical concerns of toroidal drifts on the plasma and microwave power accessibility to the resonance zone and coupling are briefly discussed. Some theoretical predictions, for ECR preionization, by Peng et al.[15] are reviewed. Relevant experiments in the literature are summarized for historical perspective.

Chapter 4 discusses the achievement in the Tokapole of lower startup V_1, volt-second consumption, runaway electron production, and impurity radiation, in light of a zero-dimensional model. Similar research elsewhere is briefly reviewed and critiqued with reference to Tokapole results.

Conclusions and suggestions for future work are presented in Chapter 5.

In this thesis, references will by made to PLP reports. These internal reports, of the University of Wisconsin Plasma Physics Group, are available on request from:

Plasma Physics Department
University of Wisconsin
1150 University Ave.
Madison, WI 53706

References for Chapter 1

[1]L.A. Artsimovich, Nuclear Fusion, 2, 215, (1972). H.P. Furth, Nuclear Fusion, 15, 487, (1975). J. Sheffield, Proceedings of the IEEE, 69, 885, (1981).

[2]J.M. Rawls, et al., "Status of Tokamak Research,"DOE/ER-0034, U.S. Dep. Energy, Washington, DC, (1979). unless otherwise specified.

[3]R.J. La Haye, et al., Nuclear Fusion, 21, 1425, (1981)

[4]J.F. Benesch, University of Texas Ph. D. Thesis (1981).

[5]A.P. Biddle, R.N. Dexter, R.J. Groebner, D.J. Holly, B. Lipschultz, M.W. Phillips, S.C. Prager, J.C. Sprott, Nuclear Fusion, 19, 1509 (1979).

[6]R. Papoular, Nuclear Fusion, 16, 37. (1976).

[7]T. Somentani, N. Fujisawa, Plasma Physics, 20, 1101, (1978).

[8]R.J. Hawryluk and J.A. Schmidt, Nuclear Fusion,16, 775 (1976).

[9]D.F.H. Start, Nuclear Fusion, 23, 1411, (1983).

[10]J.G. Cordey, Plasma Phys. and Controlled Fusion, 26, 1A, 123, (1984).

[11]A.M. Howatson, An Introduction to Gas Discharges, Pergamon Press Ltd., (1965).

[12]A. von Engel, Electric Plasmas: Their Nature and Uses, International Publications Service Taylor and Francis Inc., (1983).

[13]D.J. Rose, M. Clark, Plasmas and Controlled Fusion, The M.I.T. Press and John Wiley and Sons, Inc., (1961).

[14]J.R. Drake, Plasma Phys. and Controlled Fusion, 26, 387, (1984).

[15]Y-K. M. Peng, B.K. Borowski, and T. Kammash, Nuclear Fusion, 18, 1489, (1978).

CHAPTER 2

Experimental Apparatus

2A. Tokapole II

The experiments reported in this thesis were carried out with the Tokapole II tokamak, shown in Figure 2-1.[1] Tokapole II has a toroidal, aluminum vacuum chamber of major radius 50 cm and a 44 cm by 44 cm square cross section, as shown in Figure 2-2. The walls are 3 cm thick to limit field soak in during the 15 ms pulse. Insulated gaps allow the magnetic fields to enter the machine.

Four internal conductors are inductively driven by the iron core transformer with total available flux of 0.15 webers. A 7.2 mF, 5 kV (90 kJ) capacitor bank with a 40:1 turns ratio on the transformer produces the sinusoidal gap voltage of half-period 5.6 ms. An active crowbar is available and has a 450 V, 0.96 F (97 kJ) capacitor bank. The internal conductors (divertors) serve to shape the tokamak cross section and to divert the tokamak edge flux. The divertors have a diameter of 5 cm and are made of a chromium-copper alloy. They are supported by rods made of a beryllium-copper alloy. Each divertor has a magnetic null and x-point region associated with it. There are three plasma regions formed by this configuration. The diverted flux is

Figure 2-1. The Tokapole II tokamak with a graduate student for scale.

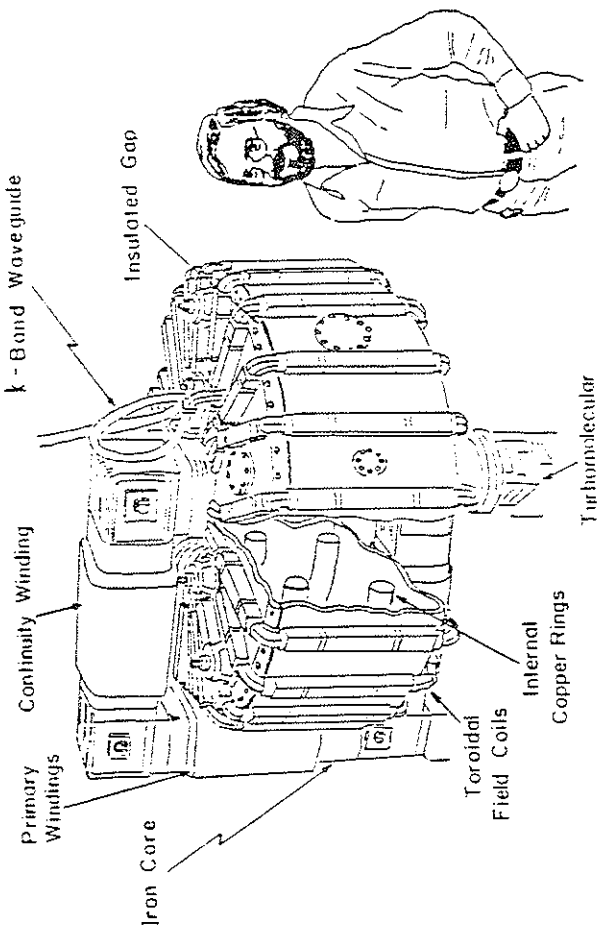

Figure 2-2. Tokapole II dimensions with representative limiter plate shapes. Dimensions are in cm.

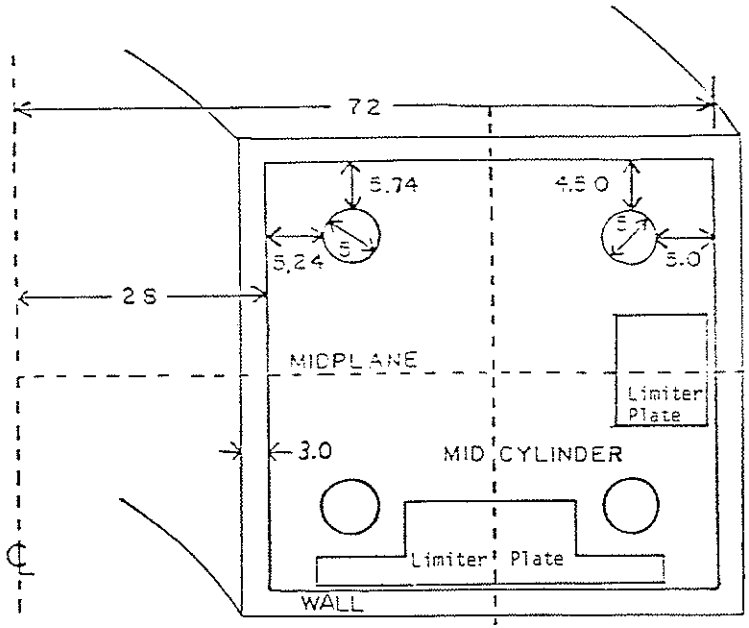

called the common flux as it encircles all four conductors and the plasma. Each divertor and the plasma has a private flux region. A four-null separatrix divides these regions (Figure 2-3).

The toroidal field, B_t, is produced by 24 sets of four wires. The wires cross the toroidal gap at uniform intervals to minimize field errors. Image currents driven in the conducting wall compensate for the spacing of the windings and improve the uniformity of the B_t. The toroidal field is driven by a 52 mF, 5 kV (650 kJ) capacitor bank and is passively crowbarred. The half-period is 10 ms.

A typical Tokapole II shot begins with the triggering of a Veeco, piezoelectric puff valve. A 10.6 ms delay allows the gas to spread uniformly around the torus. The toroidal field is pulsed, and 5.7 ms later microwaves are injected to preionize the fill gas. Five hundred microseconds pass before the transformer primary is triggered. The divertors and plasma form the secondary. A poloidal magnetic field is generated. The toroidal field peaks and is crowbarred 3-4 ms later. The time sequence is shown in (Figure 2-4).

Magnetohydrodynamics[2] predicts the plasma pressure gradient will be perpendicular to the plasma current density, J_p, and the magnetic field, B.

Figure 2-3. A theoretical poloidal magnetic flux plot.

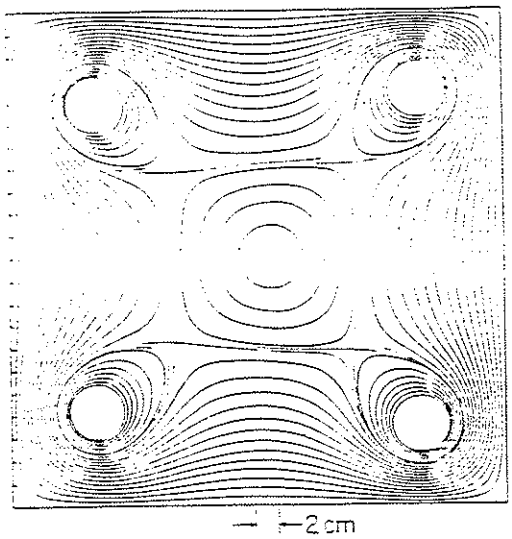

Figure 2-4. Time sequence of a Tokapole II discharge.

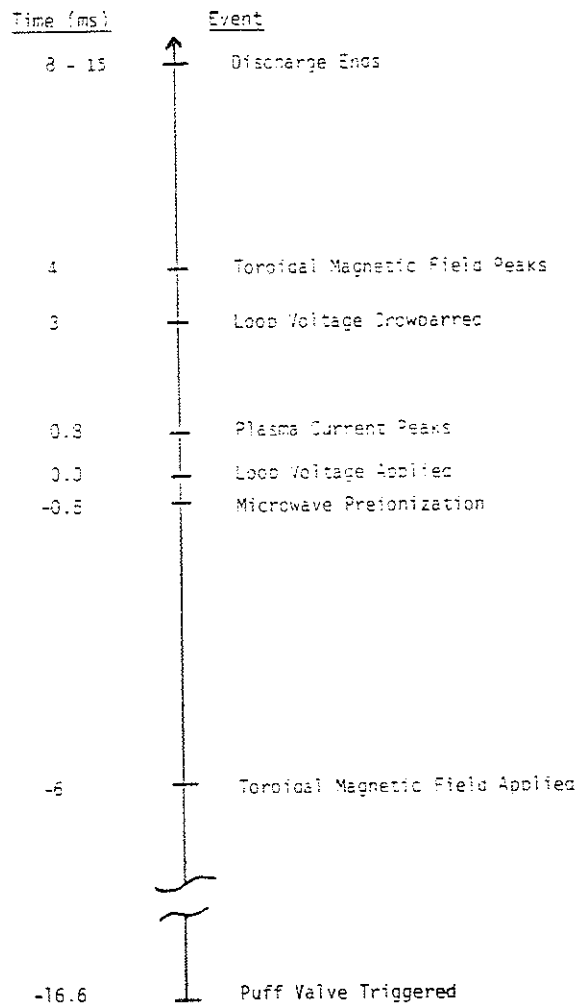

$$\nabla p = J_p \times B \qquad (2.1)$$

Consequently, the helical field lines will trace out nested surfaces of constant pressure. The nested nature of these surfaces is represented by contour plots of the poloidal magnetic flux produced by probe measurements[3] and superimposed on a theoretical plot, like that in Figure 2-3 (Figure 2-5). Presumably a contour plot of the pressure, $p \sim nk(T_e+T_i)$, would give similar results. Here n represents particle density, T_e is the electron temperature and T_i is the ion temperature. A plot of the ion saturation current to a langmuir probe demonstrates this nested nature. The experimental data are superimposed upon a theoretical poloidal flux plot (Figure 2-6). The probe signal is proportional to the product of the electron density and the square root of the temperature. The plot may be considered a first approximation to a plasma pressure profile. The relatively straight vertical contours represent the diverted flux and separatrix region.

Examination of the x-point region yields similar results. Poloidal flux probe measurements thus verify the theoretical plot (Figure 2-7a). Ion saturation current contours also agree with the theoretical flux plot (Figure 2-7b).

Figure 2-5. The plasma current poloidal magnetic flux contours measured by a probe[3] and superimposed on a theoretical flux plot.

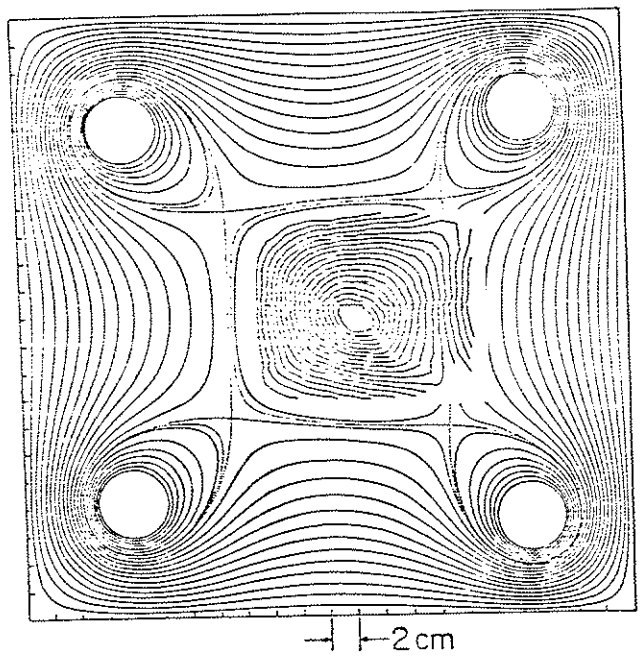

Figure 2-6. Langmuir probe ion saturation current contours of a Tokapole discharge superimposed on a theoretical poloidal magnetic flux plot.

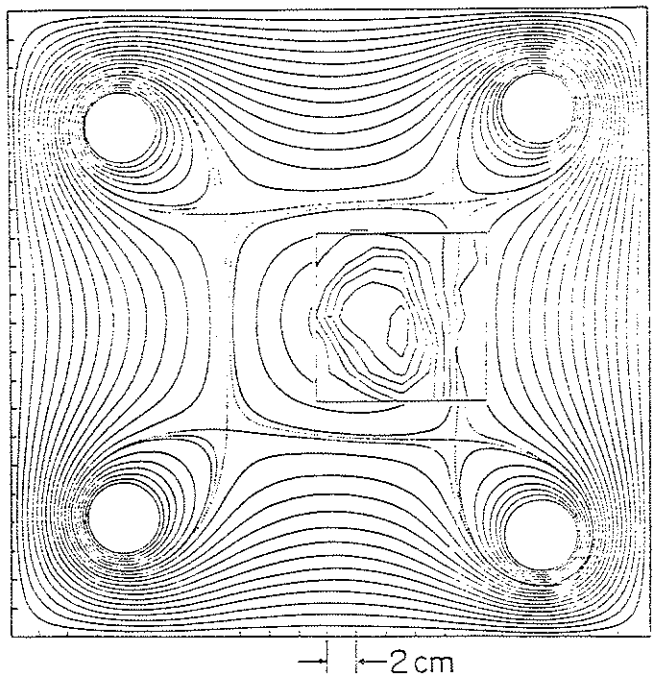

Figure 2-7. Theoretical poloidal magnetic flux contours, with probe measured contours superimposed, near the x-point. (a) Magnetic flux contours. (b) Ion saturation current contours.

a.

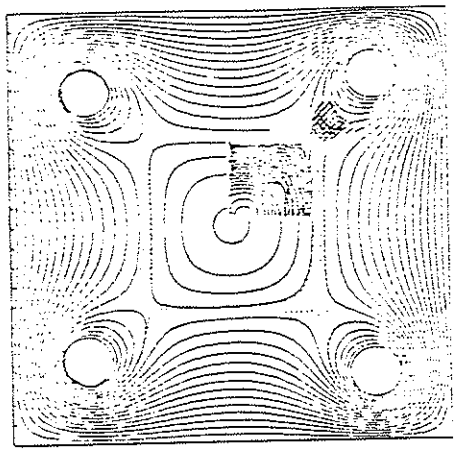

b.

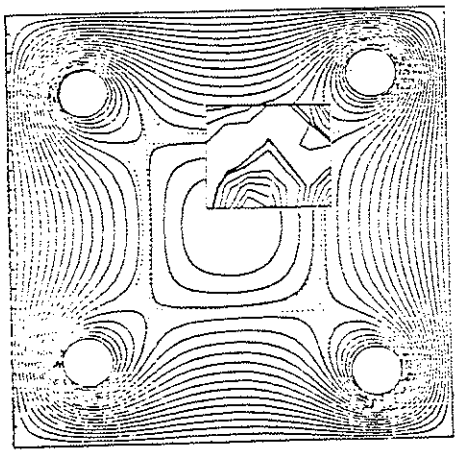

A set of four retractable limiters has been installed, as shown in Figure 2-2. The cross-section of these stainless steel plates intersects the toroidally-directed plasma current. They serve as unpumped neutralizer plates. Presently the plates intersect the diverted plasma and not that in the private flux regions. Liquid-nitrogen-cooled, zeolyte filters have been installed near the piezoelectric puff valves. Glow discharge cleaning with H_2 at 50 mtorr and 60 Hz is used nightly. The glow is sustained by an ac voltage between the internal conductors and the walls. A dc offset insures adequate bombardment of the larger wall area. A retractable Titanium getter is also available. An improved pulse discharge cleaning system will be installed by late 1984.

Data aquisition is now handled by a PDP 11/24 with a CAMAC crate of LeCroy 8210, 10 bit digitizers. A TRS-80 model I microcomputer replaced 16 channels of storage scopes for monitoring slowly changing discharge and external circuit parameters.[4] A second TRS-80 with 16 channels has been installed for spectroscopic purposes.

2B. Preionization Plasma Sources

The available microwave magnetrons operate in the s, x, and k_u bands. Frequencies of operation are 3, 9, and 15.5 GHz, respectively. The corresponding resonant magnetic fields are

easily computed from 2.8 GHz/kG. A 50 W, cw, s-band source operates during the rise of the toroidal field. This produces a small but useful electron population. The k_u-band source provides up to 12 kW for 500 μs and is the primary source for this investigation.

The k_u-band pulse has an adjustable length. A set of delay lines serves as a voltage pulse forming network (Figure 2-8). The maximum number of joules extracted from the magnetron is roughly constant. The pulse length and power output is monitored with calibrated diodes through 65 dB of attenuators. The diodes and attenuators were calibrated against a Hewlett Packard 432A power meter.

A second k_u-band magnetron is used for several experiments. A less flexible delay line network was available to drive it.

An oscillator built by A.P. Biddle provides second harmonic ICR power to heat a standard tokapole II discharge.[5] About 10 kW of the oscillator's potential output is used to aid startup.

An alternative plasma source has been constructed by A.W. Leonard. A Marshall coaxial plasma gun is now used for refueling and startup studies (Figure 2-9).[6] A stationary supply charges a mobile capacitor bank. The bank is triggered by a spark gap or a class D ignitron. A flexible transmission line carries the voltage (5-15 kV) to the gun which is mounted either

Figure 2-8. Schematic of the magnetron pulsing circuit.

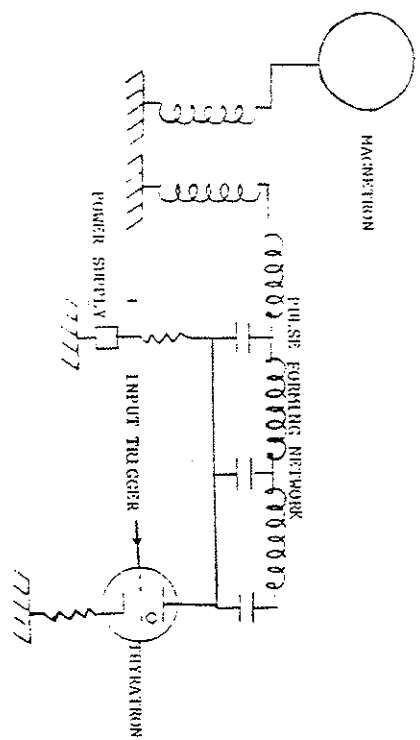

Figure 2-9. Marshall coaxial plasma gun.[7]

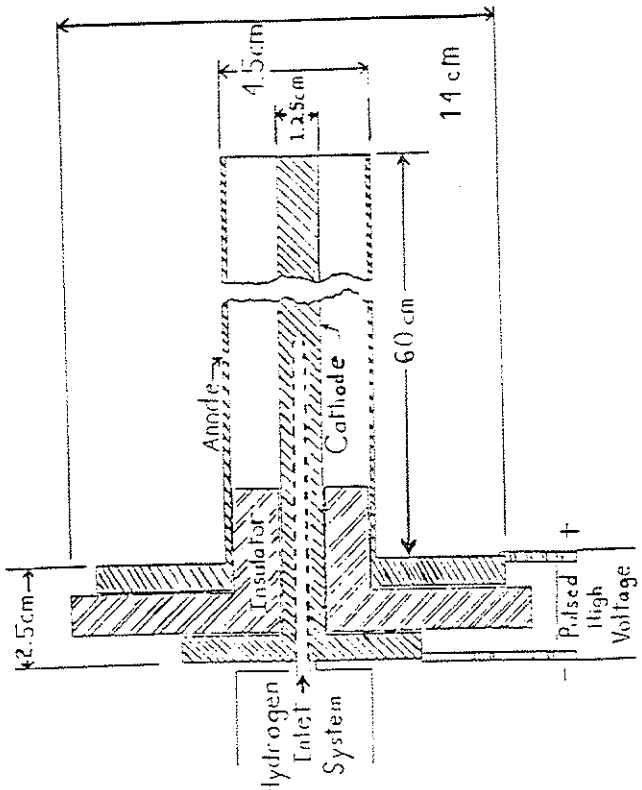

perpendicular or at 30° to the toroidal direction on the midplane.

2C. Tokapole II Modifications

The toroidal V_1 waveform has undergone major modifications. The original quarter-sine wave now has an overdamped option, which has become the standard (Figure 2-10a). A power-crowbar first option has also been developed. This applies a maximum of 8 V to the poloidal gap until the main poloidal field is pulsed (Figure 2-10b). The main field pulse has a rise time of 300 μs for this option. The rise time results from an inductor installed to protect the crowbar diode stack from the rapid dI/dt when the main field fires. A series resistance was added to damp early and late ringing of the circuit (Figure 2-11). A two-pulse poloidal field option was also developed. The capacitor bank was rewired into two separately triggerable entities. The first pulse was followed by the crowbar and then the second bank pulsed. The option to charge the half banks to different voltages should be operational in late 1984. Many tokamaks use a fast, high voltage bank followed by a sustaining bank at a fraction of the fast bank voltage. This experiment would allow the second bank to be the high voltage one.

Figure 2-10. Toroidal loop voltage waveforms available. (a) Solid line represents the cosine option. Dashed line is the damped option. (b) The power crowbar first alternative. The time delay between the crowbar and the high voltage pulse is adjustible. If the delay was long enough for the total divertor current to reach > 100 kA, discharge breakdown was inhibited.

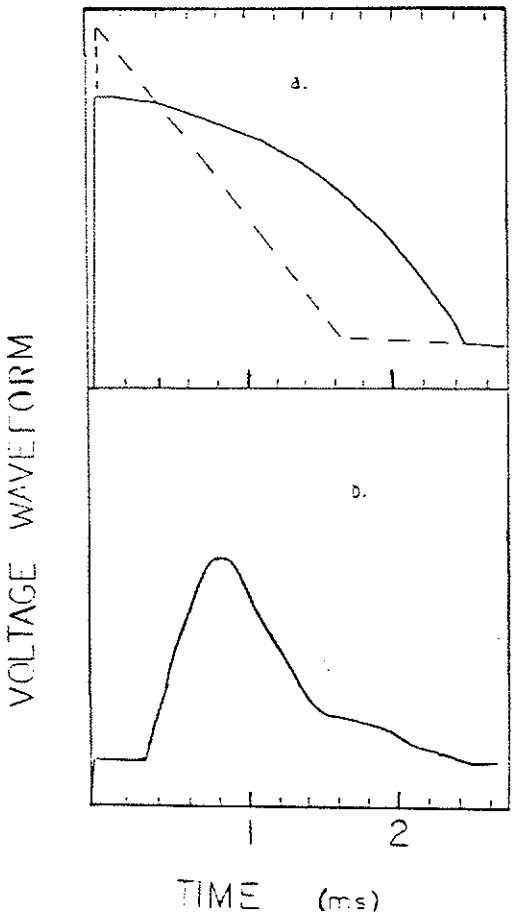

Figure 2-11. Schematic of the circuit options for the voltage waveforms shown in Figure 2-10. The knife switches are remotely operated.

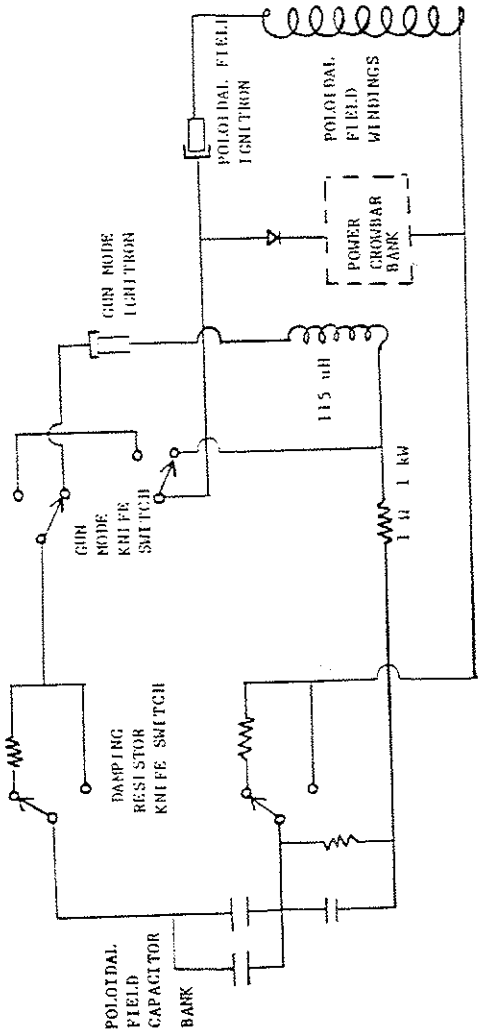

The tokamak discharge has a net expansive force along the major radius. This is due to poloidal field pressure and partly to plasma pressure. Historically, a thick conducting shell was often used to compensate for this motion. Image currents in the shell would result from plasma motion, and a vertical field would result. These image currents decay resistively, limiting their effectiveness. Initial operation of Tokapole II relied on the aluminum vacuum vessel and the poloidal magnetic field of the divertors for plasma positioning. The walls are continued topologically outside the transformer to permit uninterrupted image currents to circulate.

The successor to the thick conducting shell has been an externally generated positioning field (often a set of vertical field coils). The position control is often modified during a discharge by preprogramming or by feedback from magnetic coils sensing the plasma motion. A set of dc vertical field coils has been installed. The coil sets are 80 cm in radius and are located ±30 cm from the midplane. Both coils have ten turns. A welding supply is used to drive up to 300 amps/turn. A variable resistor allows unequal currents in the coil sets. A single coil of 10 turns was wound to produce an axisymmetric field error.

The insulation of the supports of the internal conductors has been modified to allow individual biasing to ± 10 kV. This has allowed some studies of electrostatic boundary effects on the

plasma. The conductors were also exploited as unshielded antennae for the early shear Alfven resonance experiments in Tokapole II.

2D. Diagnostics

Tokapole II has a 72 GHz interferometer, for line-average, density measurements. Impurity radiation is monitored by filtered photomultiplier tubes and several grating instruments.[7] An array of seven uncalibrated soft x-ray (SXR) detectors at one side azimuth is supplemented by similar detectors spread toroidally. Similar detectors may be mounted on swiveling probe ports. The SXR detectors are sensitive from 30 to 200 eV photon energies. A hard x-ray (HXR) detector on the midcylinder is sensitive above 1 keV. The vacuum is diagnosed by ion gauges and a residual gas analyzer. The current is deduced by a circuit which monitors the poloidal gap voltage and the primary winding current[4]. A superheterodyne, electron cyclotron second harmonic detector has also been built. A charge exchange analyzer has been used to measure T_i.

Apart from these diagnostics, all information comes from probes. The toroidal loop voltage, V_l, is measured by a probe consisting of a wire loop. Figure 2-12 schematically demonstrates the operation of this probe. The probe is inserted

Figure 2-12. Representation of the operation of the loop voltage measurement. The probe intercepts a portion of the time-changing flux outside the toroidal loop of interest. When multiplied by a geometric factor, the probe voltage is subtracted from the vertical-cut gap voltage. The gap voltage measures the time changing total flux in the machine. Consequently, the difference is the toroidal loop voltage.

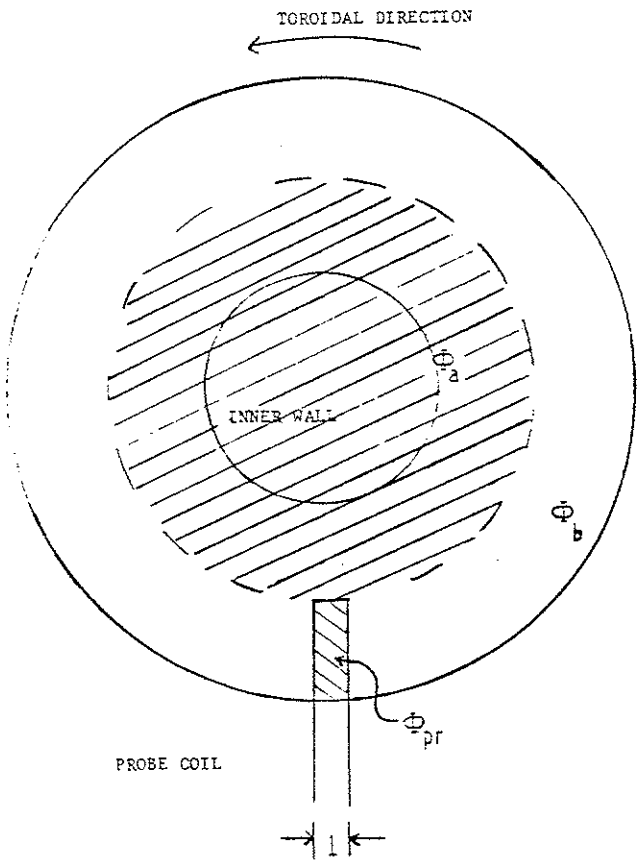

to the center of the machine. The probe voltage, V_{pr}, is proportional to the time derivative of the intercepted flux, $d\Phi_{pr}/dt$. The core flux, Φ_c, is the total flux in the machine and is the sum of the flux generating the V_l, Φ_a, and the flux outside the voltage loop, Φ_b. The Tokapole gap voltage, at the vertical cut, is the time derivative of Φ_c. Thus,

$$V_{pr} = n \frac{d\Phi_{pr}}{dt} \qquad (2.2)$$

where n is the number of windings in the probe. Thus,

$$\frac{d\Phi_b}{dt} = \frac{c}{l}\frac{d\Phi_{pr}}{dt} \qquad (2.3)$$

where c is the circumference of the voltage loop and l is the length of the wire loop along the voltage loop. The gap voltage is given by

$$V_{gap} = \frac{d\Phi_c}{dt} = \frac{d\Phi_a}{dt} + \frac{d\Phi_b}{dt} \qquad (2.4)$$

or

$$V_l = \frac{d\Phi_a}{dt} = V_{gap} - \frac{cV_{pr}}{l\,n} \qquad (2.5)$$

So measurement of the gap and probe voltages yields the toroidal loop voltage. The design value of the diverted flux without plasma is one half of the core flux and has been verified with this probe. Hence, the plasma will experience roughly half the gap voltage.

Single, double and triple tipped probes[8,9,10] have been used to determine local plasma potential, density, and temperature, respectively. The floating potential, V_f, is the voltage across a high impedance termination of the probe. Local density measurements are made with a probe biased into the ion saturation current, I_s, region of the current voltage, I-V, characteristic. The expression for ion density, n_i, is:

$$n_i = \frac{4I_{si}\left[\pi m_i\right]^{1/2}}{Ae\,(8kT_e)^{1/2}} \qquad (2.6)$$

A is the probe tip area and m_i the ion mass. The formula is valid if $T_i < T_e$. To determine n_i from this one needs T_e. A voltage sweep from I_s to electron current saturation traces out the complete I-V plot. The slope at V_f is related to T_e:

$$\left(\frac{dI}{dV}\right)_{V_f} = \frac{eI_s}{kT_e} \qquad (2.7)$$

In practice, a triple probe may be used to give T_e without obtaining the I-V characteristic.[10]

$$\frac{kT_e}{e} = \frac{(V_1 - V_2)}{\ln\left(1 + \frac{A_3}{A_1}\right)} \qquad (2.8)$$

The subscripted V and A quantities refer to the bias voltage and area of a tip, ($V_2 = V_f$). The admittance[11] probe has also been used for temperature measurements. The above expression for dI/dV at V_f is the reciprocal for the sheath resistance, R_s, of the probe plasma interaction zone. This sheath admittance is measured by a capacitance bridge balanced to read zero with no plasma present. An oscillator drives a sinusoidal waveform with amplitude $\delta V < kT_e/e$ and frequency, f, such that $f < f_{pi}$. f_{pi} is the ion plasma frequency, and this restriction insures resistive rather than reactive response. Circuit response is calibrated against known resistances, and I_s is usually measured simultaneously.

$$\frac{kT_e}{e} = R_s I_s \qquad (2.9)$$

The three temperature measurement techniques agree in the microwave preionization afterglow plasma. While the microwave power is injected, the triple probe gives the most unambiguous and reproducible result.

Small magnetic pick-up coils have been used to map the poloidal flux plot, observe rf resonances in the plasma, and to study magnetic fluctuations. Scintillator probes, provided by Professor R.N. Dexter, have been used to detect high energy electrons. A piece of scintillator plastic is enclosed in the tip of a stainless steel tube. The plastic is shielded from the plasma environment by either the tube wall or an adjustable number of aluminum foil layers. A small rogowski coil, constructed by B. Lipschultz, has been used for current profiles in the diverted region. A retractable rogowski loop which encircles the tokamak flux surfaces has been used to verify the accuracy of the current monitor circuit. A rogowski loop measures current via the magnetic flux passing through its poloidal windings.

$$I = \frac{\phi}{\mu_o NA} \qquad (2.10)$$

Where ϕ is the flux through the coil, N the number density and A the area of the turns. A passive integrator attached to the output gives:

$$V = \frac{1}{RC} \int_o^t \frac{d\phi}{dt} dt = \frac{NA\mu_o I}{RC} \qquad (2.11)$$

Note that in regions of the large poloidal field gradients, due to the internal conductors, the baseline of the rogowski signal will be distorted by flux pick up not of toroidal current origin.

Another method of measuring plasma current is the double-tipped saturation probe. The tips are insulated from each other. A differential amplifier with adequate CMRR gives the difference of the saturation currents which is the plasma current.[13]

The probe data below is primarily from the preionization plasma, early startup and edge measurments in the diverted flux. In general for these measurements, $T_e < 60$ eV, and very low current density regions are intercepted. Under these conditions, the probes have little effect on the plasma.

References for Chapter 2

[1]A.P. Biddle, et al., Nuclear Fusion 19, 1509 (1979).

[2]G. Bateman, MHD Instabilities, The MIT Press, (1978)

[3]B. Lipschultz, Nuclear Fusion 20, 683, (1980).

[4]J.C. Sprott, University of Wisconsin Plasma Studies PLP 889 (1983).

[5]A.P. Biddle and J.C. Sprott, Plasma Physics 23, 679, (1981).

[6]A.W. Leonard, R.N. Dexter, A.G. Kellman, J.C. Sprott, Bull. of the Am. Phys. Soc. 28, 1149 (1983).

[7]R.J. Groebner and R.N. Dexter, Plasma Physics 23, 693 (1981).

[8]F.F. Chen, in Plasma Diagnostic Techniques (R.H. Huddlestone and S.L. Leonard, eds., Academic Press, 1965), Chapter 4.

[9]J.C. Sprott, University of Wisconsin Plasma Studies PLP 88 (1966).

[10]J.F. Etzweiler, Ph.D. Thesis, University of Wisconsin (1977).

[11]J.C. Sprott, Rev. Sci. Instrum. 39 1569 (1968).

[12]D.E. Lencioni, Ph.D. Thesis, University of Wisconsin (1969).

Chapter Three

Preionization Plasma in a Toroidal Magnetic Field

Plasma behavior in a purely toroidal magnetic field is crucial to understanding the power balance of an ECR plasma in a tokamak. Other methods of preionization plasma production are subject to the same toroidal physics. Tokapole II results indicate warm electrons, 50 eV $\leq T_e \leq$ 1 keV, dominate the power balance of the ECR plasma, while the microwave power is applied. The existence of the warm electrons is deduced from measurements of a vertical electric field ($E_v \sim T_e/2a$) and of the vertical current due to drifts. The E_v is non-negligible despite the low resistance path provided by the vacuum vessel, contrary to the shorting-out assumption of some authors.[1] The vertical current, due to drifts, is ten times the current anticipated from the bulk ECR plasma. The vertical current losses may account for most of the injected power.

First, the effects of toroidicity on the plasma are briefly discussed. Plasma formation mechanisms and access to resonances are discussed but are not of prime interest to the experiment. A model for the ECR plasma in a purely toroidal field is briefly reviewed. Experiments by other investigators are discussed before Tokapole II results are presented. The approximate power

balance of the microwave-power-on, ECR plasma is presented with reference to the impact on larger devices.

3A. Theoretical Considerations

3A1. Effects of a Toroidal Magnetic Field on a Preionization Plasma

The single particle drifts of a plasma in a toroidal field are derived in standard texts.[2] The 1/R decline of the toroidal field produces drift due to ∇B. The curvature of the toroidal field produces a drift, due to centripetal acceleration. Both drifts result in vertical charge separation of the same sense. A vertical electric field, E_v, develops and causes an $E_v \times B_t$ drift radially outwards. This drift is charge independent.

Compactly stated:

∇B and Curvature drift:

$$v_d = \frac{m}{q}\left(v_{\parallel}^2 + \left(\frac{1}{2}\right)v_{\perp}^2\right)\frac{R_c \times B}{R^2 B^2} \qquad (3.1.a)$$

For estimates of confinement time, it is convenient to use the curvature drift in the following form:

$$v_c = \frac{2kT_e}{eRB_t} \qquad (3.1.b)$$

where $2kT_e = m_e v_f^2$. Since equation 3.1.b uses $n_e kT_e$ instead of $(3/2)n_e kT_e$, it overestimates purely VB drift (by 25%) and underestimates purely curvature drift (by 30%), but is commonly used in the literature as an estimate of drift from both sources. v_c is termed the curvature drift.

$\underline{E_v \times B \text{ drift:}}$

$$v_e = \frac{E_v \times B}{B^2} \qquad (3.2)$$

A study done before the ISX-B experiment[3] assumed E_v to be small for the power balance. The justification assumes that a 1 mΩ vacuum vessel resistance from the top to the bottom shorts out E_v. The vertical current due to drifts is estimated to be 900 Amps for a 250 eV plasma of 3.2×10^{12} cm^{-3} density.[1] The estimate assumes uniform T_e and n_e over the volume with curvature drift, such that $v_c = 3.85 \times 10^4$ cm/s. Assuming the vessel resistance limits the vertical voltage, ohm's law gives a vertical voltage of $V_v = 0.9$ V. The vertical distance is 54 cm, and so $E_v = 0.02$ V/cm. The resultant E_v crossed with B = 12 kG gives an insignificant radial velocity (about 170 cm/s).

Another argument against $E_v \times B_t$, as a significant loss channel, is made in reference 4. Assuming the drifts are charging plates of infinite impedance, the vertical electric field is limited by the particle energy. If a particle, drifting towards the plate, is unable to pass through the potential gradient, it will not contribute to the charging process. Thus, Borowski, et al. write the $E_{maximum} \times B$ confinement time as:

$$\tau_E = \left[\frac{(\Delta R_{uh}\, m_i)}{k(T_e + T_i)}\right]^{\frac{1}{2}} \qquad (3.3)^4$$

where Δ, the ECR-UHR separation, is the plasma radial scale length used, R_{uh} is the UHR radius (=R), and m_i is the ion mass. This gives $\tau_E = 4.8$ μs and an $E_v \sim 3 \times 10^2$ V/cm for ISX-B. Roughly 30 times the available ECR power would be needed to sustain the plasma.

Further analysis of both arguments is productive. The vessel resistance method ignores an element of the system, the plasma-sheath resistance. The infinite impedance plate approach gives a maximum E_v independent of boundary conditions. Assume the $\sim 10^2$ V/cm, from the infinite impedance plate method, is the upper limit for the plasma E_v. Next, consider the sheath resistance of the plasma in series with the vacuum vessel. This resistance limits the maximum E_v which could be sustained by the

plasma, sheath, and vacuum-vessel system. The following expression describes the sheath resistance of a probe collecting ion saturation current in a plasma[5], but is used to provide an order of magnitude estimate for a metallic boundary of the plasma exposed to a drift current.

$$R_s = \frac{T_e}{j_{oi}A} \qquad (3.4)$$

R_s is the sheath resistance, and $j_{oi}A$ is the ion saturation current density times the area of the collecting surface. Using the vertical current, I_v, in place of I_s ($= j_{oi}A$) and Ohm's law ($R_s I_v = 2aE_v$), this argument is equivalent to $E_v \sim T_e/(2a)$, but is expressed in terms of a resistance as an intuitive aid.

Using the ISX-B parameters calculated in reference 1, of T_e = 250 eV and vertical current, I_v, equal to 900 Amps, $R_s = 0.28\ \Omega$ and $E_v \sim 5$ V/cm. Thus, the E_v supported by the sheath resistance is less than that calculated from the infinite impedance charging method and is much greater than that with the vacuum vessel resistance limiting the maximum value. A B_t of 13.5 kG implies the $E_v \times B_t$ drift velocity is 3.7×10^4 cm/s. This is on the order of the curvature drift. This estimate suggests a significant vertical electric field could be sustained. The model of Peng, Borowski, and Kammash is discussed further in section 3A3.

The comparison of these predictions to experiment is presented in sections 3B., for ISX-B, and 3C., for Tokapole II.

3A2. Accessibility and Coupling of ECRF to the Preionization Plasma

Any startup plasma will be subjected to the above toroidal effects. In the case of ECR generated plasma, accessibility of the interaction region and the coupling mechanism must also be considered.

The propagation of electromagnetic waves through a magnetized plasma is crucial to ECR preionization. Plasma regions which are capable of absorbing the power must be accessible from the launching structure. The first approximation of accessibility comes from cold plasma theory for a slab.[6] The Fourier-Laplace transformed Maxwell's equations give a tensor dispersion relation:

$$\underline{k} \times (\underline{k} \times \underline{E}) + \frac{\omega^2}{c^2} \underline{\underline{\varepsilon}} \cdot \underline{E} = 0 \qquad (3.5)$$

Where $\underline{k}$ is the wave vector, $\underline{E}$ the electric field propagating at frequency, ω, and $\underline{\underline{\varepsilon}}$ is the dielectric tensor. In toroidal geometry, the desired waves propagate perpendicular to the indigenous magnetic field, ($\underline{k} \perp \underline{B}$). For $\underline{E}$ perpendicular

(parallel) to $\underline{B}_t$ the wave is termed extraordinary, X, (Ordinary,O).

The indicies of refraction for perpendicular incidence of the X and O modes may be written:

$$n_O = 1 - \Pi^2 \qquad (3.6)$$

$$n_X = 1 - \Pi^2 \frac{1 - \Pi^2 - \Omega_+\Omega_-}{(1 - \Omega_-^2)(1 - \Omega_+^2) - \Omega_-\Omega_+} = 2\frac{K_r K_l}{K_r + K_l} \qquad (3.7)$$

The K's are components of the dielectric tensor in a rotating coordinate system. K_r (K_l) gives the cutoff condition for a right (left) circularly polarized wave propagating along the magnetic field. The two polarizations of the extraordinary wave satisfy the form of the cutoff conditions of parallel propagation despite the fact of perpendicular propagation. The ratio of the plasma ($\omega_{pe} = (n_e e^2/\varepsilon_o m_e)^{1/2}$) to incident frequency (ω_o) is:

$$\Pi = \frac{\omega_{pe}}{\omega_o} \qquad (3.8)$$

The ratios of the electron and ion cyclotron frequencies ($\omega_{ce,ci} = eB/m_{e,i}$) to the incident frequency are represented by Ω_- and Ω_+

respectively.

$$\Omega_- = \frac{\omega_{ce}}{\omega_o} \qquad (3.9)$$

$$\Omega_+ = \frac{\omega_{ci}}{\omega_o} \qquad (3.10)$$

Plasma cutoffs occur for zero values of the indicies of refraction, and resonances occur for infinite values.

O-cutoff:

$$\Pi^2 = 1 \qquad (3.11)$$

X-cutoff:

$$\frac{(1 - \Pi^2 - \Omega_-\Omega_+)^2}{(\Omega_- - \Omega_+)^2} = 1 \qquad (3.12)$$

or: $K_r K_l = 0$

X-resonance

$$(1 - \Sigma^2)(1 - \Omega_+^2) - \Pi^2(1 - \Omega_-\Omega_+) = 0 \qquad (3.13)$$

If the ion terms are set to zero the UHR is defined as:

$$\omega_{uh}^2 = \omega_{pe}^2 + \omega_{ce}^2 \qquad (3.14)$$

There is no O-mode resonance in cold plasma theory.

In the toroidal geometry of the tokamak, the magnetic field falls as 1/R, where R is the radius. Thus microwaves launched from the outside of the torus experience increasing B_t as they propagate. Such a field gradient sets limits on the accesibility of resonance zones. Launch from this low field side (LFS) is convenient for mechanical reasons, which include the transformer at the inner wall. The following discussion focuses on LFS launch.

For brevity, the discussion is restricted to microwave (15.5 GHz) propagation from the low field side, through a Tokapole plasma with $n_e > 1 \times 10^{11}$ cm^{-3}. At this density the X-mode is cutoff one half wavelength radially out from the ECR. This cyclotron cutoff is shown in the CMA diagram in Figure 3-1[2] as a dashed boundary. The microwaves are launched with arbitrary amounts of O and X modes. The X-mode components are reflected from the plasma towards the outer wall.

The O-mode from the LFS then has two sources. These are the launched microwaves and the O-mode waves created by X-mode reflection from the outer wall. The O-mode is not cutoff as the

Figure 3-1. A Clemmow-Mullaly-Allis diagram showing the right hand (R) cutoff as a dashed line separating the low magnetic field and low density region from the UHR and ECR.

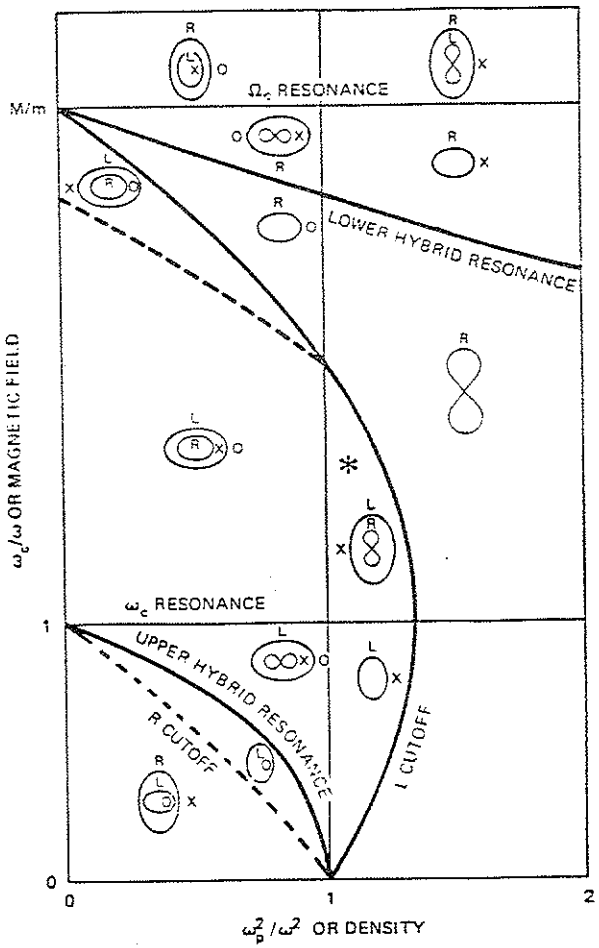

density is not high enough (eq. 3.11). The O-mode which reaches the inner wall is reflected and may convert to an X-mode upon reflection. The portion of the microwave power which is reflected from the inner wall as X-mode radiation propagates freely to the ECR and is absorbed.

The rising plasma density separates the ECR and UHR layers (eq. 3.14), and alters the X-mode polarization to left circular as it propagates from the inner wall. Physically[7], this is due to a polarization of the plasma caused by the finite wavelength of the wave along the axis of the wavevector. The displacement of the electrons with respect to the stationary ions is equal to the gyroradius, r_g. The polarization field is twice the applied field and in the opposite direction. The left circular polarization cannot interact at the ECR layer and passes through to the UHR layer.

At the UHR, theory indicates the X-mode converts [8] to an electrostatic plasma wave, the "electron Bernstein mode". The Bernstein wave is absorbed by the electrons, via Landau damping. Mode conversion in addition to ion acoustic waves, has also been observed. [9]

To model experimental results, Anisimov, et al. [10] derive an expression to distinguish the high density regime, with conversion to left circular polarization, from the low density regime. The direction of rotation of the wave field depends on n_e, B_t, and the angle of propagation with respect to B_t, α. The condition for wave field rotation change is that $\alpha > \alpha_p$ which is determined by the expressions for the resonance criterion at the cyclotron resonance zone and α.[11]

$$\tan^2 \alpha_p = \frac{(1-\Pi^2)(1-\Omega_-^2)}{1-\Pi^2-\Omega_-^2} \qquad (3.15a)$$

α is determined from:

$$\tan^2 \alpha = \frac{1 - u - \cos^2 \alpha_o}{(1 - \frac{u}{2})\cos^2 \alpha_o} \qquad (3.15b)$$

where α_o is the angle of injection and u is defined as:

$$u = -(\Pi^2)(\frac{1}{\omega_- - 1})$$

As the wave propagates towards lower B_t, α increases due to an

increase in the perpendicular index of refraction. The result for conversion to the left-handed polarization is written as:

$$\Pi^2 > 2(\Omega_- - 1) \qquad (3.16)$$

Experimentally the left-hand side has the approximate value of 0.04.

Several experiments designed for ECR heating of the ohmically-established plasma launch the X-mode from the inner wall. [12] Heating has also been reported with O-mode launch from the LFS. [13] The former avoid the cyclotron cutoff. The latter is density limited, but within possible reactor parameters. Thus, the same delivery system for heating may be used for preionization.

3A3. A Model of the ECR Plasma in a Toroidal Field

A model incorporating the physics issues in sections 3A1 and 3A2 was formulated by Peng et al.[1]. The assumptions of the theory follow the experimental observations of references 9 and 10. The extraordinary mode is launched from the high field side. It is assumed to mode convert to electron Bernstein waves at the UHR, and the power is absorbed in a single pass.

The microwave power is restricted to prohibit the production of runaway electrons. An expression derived in reference 14 is used to estimate the perpendicular electron energy, $W_{\perp R}$, attained near the resonance zone, in the low density regime ($\Pi^2 < 0.04$).

$$W_{\perp R} = 2m_e c^2 \left[\frac{eE_o}{m_e \omega_o c}\right]^{2/3} \quad \text{(eV)} \qquad (3.17)$$

The estimate for ISX-B parameters was 5 keV. For Tokapole the microwave electric field, E_o, is 300 V/cm and $\omega_o = 9.7 \times 10^{10}$ Hz, f_o=(15.5 GHz). This gives $W_{\perp R} = 3$ keV near the ECR. Scintillator probes detect hot electrons in the Tokapole ECR plasma, which could be in the tail of a distribution function with $T_e \sim 3$ keV.

A particle balance assumes the ISX-B losses are curvature drift, and parallel loss due to field errors, δB. The authors assume the field error loss velocity (v_δ) is equal to v_i times $\delta B/B$. Comparison to curvature drift velocity gives a criterion for deleterious δB. If $\delta B > (3)^{1/2}(m_e cv)/eR = (c/eR)(6m_e T_e)^{1/2}$, the error is significant and must be included. They estimate $\delta B > .656$ G is significant and requires correction coils.

The energy balance includes ionization of neutrals, collisions with ions, impurity radiation and the particle losses, but ignores $E_v \times B_t$ drift as discussed in section 3A1. The δB chosen was 0.5 G. An estimate of $T_e = 250$ eV near the UHR is obtained, assuming 120 kW injected and $n_e = 3.2 \times 10^{12}$ cm^{-3}.

After the particle-energy balance results are obtained, ambipolar electric fields are considered to assist confinement. First, the coldness of the ions causes an ambipolar potential ($\sim T_e/e$) along field lines. Parallel losses are reduced by a factor of the square root of m_i/m_e.

The perpendicular confinement assistance is from the sheath at the wall. They assume the magnetic field allows electric field penetration to exceed the Debye length, 10^{-2}cm. Thus, an $E_{amb} \sim V_{amb} \sim T_e/(ea)$ extends into the plasma and causes an $E_{amb} \times B_t$ drift parallel to the plasma-wall boundary. This drift is poloidal in direction and neutralizes the E_v from ∇B and curvature drifts. They speculate confinement is improved and impurity influx is reduced by the $E_{amb} \times B_t$ drift. This is in analogy to the streaming of particles along helical field lines when significant plasma current is present. If the 50 eV electrons detected in the UHR layer[3] are responsible for this ambipolar field, the drift velocities would be $\sim 1.4 \times 10^4$ cm/s in ISX-B. This is the same order as the curvature drift, $v_c = 3.85 \times 10^4$ cm/s.

This theory was applied to the Fusion Engineering Device (FED) startup, with modifications due to the experimental results from ISX-B.[4] The ambipolar field drift is a major aid to

confinement, but secondary electrons from hot electron impact at metallic boundaries degrade this extended sheath effect. Using ISX-B data, $T_e \sim 10$ eV, $n_e \sim 3 \times 10^{12}$, and radiated power ~ 5 kW out of 80kW imput, the model accounts for 25% of the power input, "Even with secondary electrons". If higher T_e is assumed (UHR layer $T_e < 100$ eV, ECR layer $T_e \sim 20$ eV), the model requires 66 kW compared to the 80kW imput.

3B. Experiments on an ECR Plasma in a Toroidal Field

Experiments by Anisimov et al.[9,10,14,15] study the migration of the microwave interaction with the plasma from the ECR to the UHR. The work was done with a device of R = 21.5 cm, a = 6 cm, and B_t = 3 kG on axis. The x-band sources include one essentially cw (0.5 sec) and one pulsed (5-15 μs). Power levels are 1-200 watts and 0.1-10 kW respectively. The microwaves were launched from either the low field or the high field side of the torus. Hydrogen and argon are the working gasses. Pressures range from 10^{-4} to 10^{-3} torr.

No breakdown is recorded for pressures below 10^{-4} torr and/or below powers of 10 watts. The pulsed source launches into a quasi-stationary plasma formed by the low power, cw source. This technique eliminates ambiguities normally present with

drifts. The pulse length is less than the estimated particle lifetime.

At low density, power absorption takes place in the ECR layer. A pressure of 7×10^{-5} torr and a power of 50 kW for 150 μs produces x-rays and low frequency oscillations. The gas breaks down, and significant plasma radiation is detected. Microwave fields are detected only up to 40 cm (toroidally) away from injection, after breakdown, implying good absorption. The x-ray energy is 30-40 keV, and the oscillations had a frequency of about 200 kHz. The latter is presumed to be an ion acoustic wave and indicates mode conversion occurs near the UHR. The application of the 15 μs pulse shifts the absorption layer to the UHR, for $\omega_{pe}^2/\omega_o^2 > 0.04$. The density profile was measured with a single Langmuir probe.

The injected electromagnetic wave is assumed to decay into an "oblique plasma wave". This is consistent with the mode conversion discussed in section 3A.. When ∇n is perpendicular to ∇B, the plasma waves propagate toward higher B. Evidence of fast electron (30-40 keV), generation implies to the authors that Landau damping of the wave is the collisionless power transfer mechanism.

The pulsed source is used to study the radial drift velocity to the outer wall. For 10^{-3} torr, the measured outward drift

velocity is 1.3×10^5 cm/s. The driving mechanism is assumed to be the $\underline{E} \times \underline{B}$ drift.

Holly and Witherspoon [16] used 1-10 kW at 8.8 GHz to study a microwave plasma in Tokapole II's toroidal field. They report the density peak at the ECR layer. The densities of operation, 10^{8}-10^{10} cm^{-3} separate the ECR and UHR layers by less than 0.5 cm. This is the step size between data points. Also, the toroidal field is changing during the pulse, smearing out the resonance peak spatially.

Experiments on WT-1[17], WT-2[18], Tokapole II[19] and ISX-B[3] report similar observations. ISX-B [3] is unique, as the high power 35 GHz gyrotron has a 15 ms pulse length and launches from the high field side, at 45° with respect to a major radius line of sight. Interferometer measurements and high speed movies demonstrate initial plasma forms at the ECR (97 cm) layer and migrates to the UHR (108 cm) layer after 2 ms. An equilibrium between power in and out is established at 5 ms into the pulse. The resonance zone is smeared out between the UHR and ECR layers. Measurements of T_e confirm this picture. The plasma reaches 5×10^{12} cm^{-3} at a bulk T_e of 10 eV. An electrostatic particle energy analyzer indicates $T_e \sim 50$ eV in the UHR layer. A pyroelectric detector acts as a total radiometer and indicates the radiated power is less than 10% of that injected. The energy

balance ISX-B is not as anticipated by the theoretical analysis.[1]

A later ISX-B experiment used another gyrotron with 70 kW at 26 GHz.[20] One of the rail limiters was grounded to collect vertical-drift current. Reversal of B_t should change the sign of the current, but an asymmetry exists in the vertical current. The sign changes but so does the magnitude. The explanation given is that a field error exists of the order $\delta B/B_t \sim 1 \times 10^{-3}$. A model using $\delta B/B = 0.15\%$ and curvature drift matches the experiment, but the e-folding time of the afterglow plasma is 10 ms. This e-folding time implies $\delta B/B < 6 \times 10^{-5}$. The model does not include an $\underline{E} \times \underline{B}$ term, as the thermal electrons (10 eV) are assumed to limit the magnitude of E_v.

3C. ECR Plasma in the Toroidal Magnetic Field of Tokapole II

The power balance deduced from experiment consists of three loss terms: curvature drift, radiation, and ionization. Non-thermal, vertical electric fields and currents are measured with probes. These experiments indicate three electron temperatures are important. Very early in time (< 150 μs), hot electrons (> 10 keV) are produced near the ECR layer, but few are detected at later times. During the density plateau, warm (50 eV < T_e < 1 keV) and bulk electrons (T_e < 10 eV) may explain the power balance. The warm electrons are suggested by the measured E_v ~ 10 V/cm (~T_e(warm)/2a), the ~ 50 Amps of vertical current, and the T_e measured by a triple probe.

The qualitative behavior of the microwave plasma will be discussed first. Quantitative measurements will be presented, as the basis for section 3C6 dealing with the energy balance. The afterglow plasma decays as expected from drifts and was found sufficient for high density preionization benefits (Chapter Four). Attempts to increase the energy confinement time of the ECR plasma were made.

3C1. An Overview of the Behaviour of the ECR Plasma

The representative microwave pulse, shown in Figure 3-2, is 300 μs long. The earliest signature of the microwave power, P_μ, absorption is a burst of high energy electrons. These are detected with foil-covered scintillator probes. This signature declines as the Hβ, n_e, and impurity radiation increase.

A large, vertical floating potential gradient, ∇V_f, is observed, with probes, throughout the plasma lifetime. Initially this gradient is about 40 V/cm. As the density rises, the vertical electric field, E_v, declines and levels off until the P_μ decays. The plateau value is about 10 V/cm. Assuming E_v ~T_e/el where l = 40 cm, the electron temperature would be ~400 eV.

A vertical current, I_v, exists during this time, due to curvature drift. At the end of the P_μ pulse, I_v and E_v decay to nearly zero, within 100 μs. The afterglow plasma has a decay time consistent with drift losses.

Data runs were taken with the microwave power sagging 50% during the pulse. These plasmas flattop in density and radiation output. The power sag was reduced to 5-10% for some experiments. Those plasmas show a slight rise in density throughout the pulse. The maximum density at a particular power level was not reached, due to the limited pulse length of the sources. ISX-B reported that a pulse length > 5 ms produced an equilibrium between power in and maximum density.[3]

Figure 3-2. Representative data during a 16.5 GHz microwave pulse.

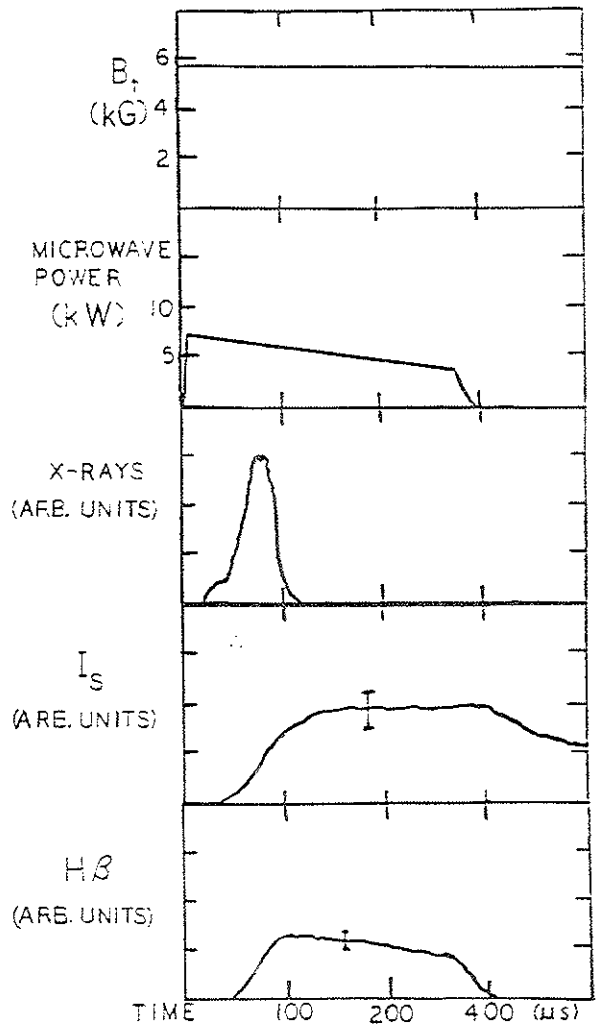

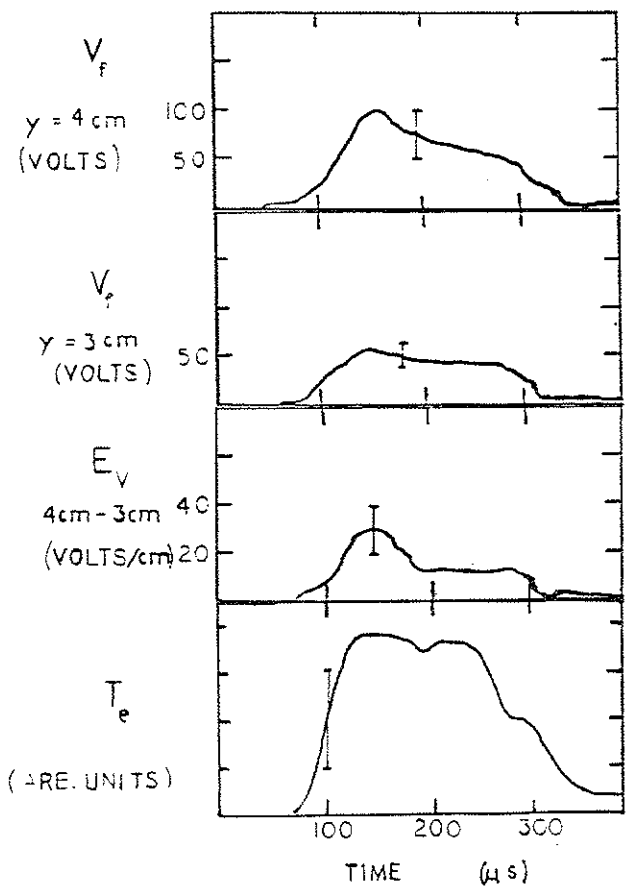

Moderate power (5-12 kW), breakdown was sensitive to pressure. Below 0.50 x 10^{-4} torr, a burst of high energy electrons was detected, but little radiation or density developed. A plot (Figure 3-3), of the time-integrated scintillator signal vs. fill pressure is compared to the ion density. The scintillator signal peaks at 0.50 x 10^{-4} torr. The density peaked at 2.5 x 10^{-4} torr, which was the fill pressure chosen for the following experiments. This corresponds to 1.6 x 10^{13} cm^{-3} hydrogen atoms.

3C2. Resonance Zone Location

The microwaves are launched from the low field side, and the cyclotron cutoff prevents E-mode penetration to the ECR. This experiment relies on multiple reflections of the sort discussed in section 3A2 to deliver the power to the resonance zone. This is roughly equivalent to launching the waves from the high field side. The conventional wisdom culled from wave theory and previous experiments indicates ECR power from the high field side will initially interact at the ECR layer. As the fill gas is ionized, the interaction at the ECR layer declines. The power passes to the UHR layer, where mode conversion takes place. No modifications are necessary to explain Tokapole II observations.

Figure 3-3. Dependance of I_s (o) and the integral over time of the hard x-ray signal (x) versus fill pressure with 10 kW at 15.5 GHz.

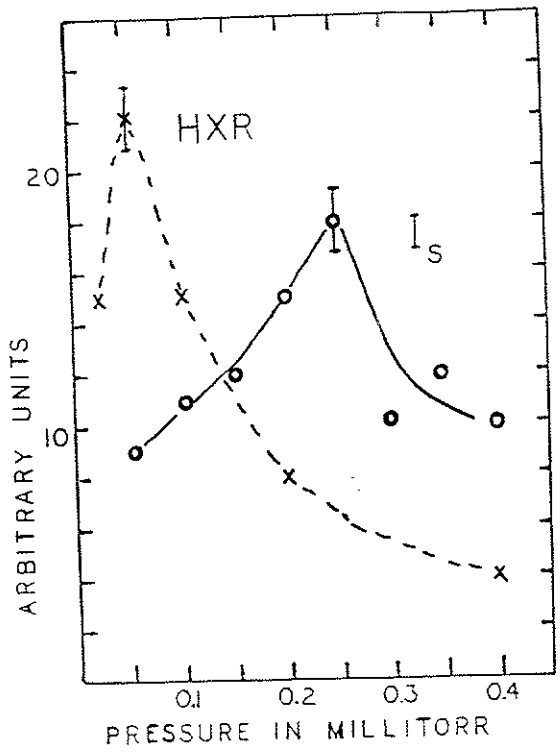

If the ECR layer is positioned beneath a foil-covered scintillator, the first detected interaction, during microwave injection, is a burst of x-rays. These are from hot electrons striking the detector foil. The burst contains electrons up to 100 keV in energy, as they penetrate 1/64" stainless steel. Since the 100 keV signal was very small, the 50 keV electrons observed with the aluminum-foil covered probes were considered in light of the result of eq. 3.16. Assuming a Maxwellian distribution with a particle temperature of 3 keV and $n_e \sim 10^{10}$ cm^{-3}, one would expect $6 \times 10^2 cm^{-3}$ electrons at 50 keV. This is consistent with the low density interaction expected, as the detected hot electrons could be the tail of a multi-kilovolt electron distribution function.

Changing values of B_t from shot-to-shot sweeps the ECR layer past a scintillator and filtered photomultiplier tubes on the midcylinder. The x-ray signal, Hβ, and impurity radiation are monitored during the sweep. An I_s radial profile was done, by moving the probe shot to shot.

An estimate of the ECR to UHR separation may be made using eq. 3.14. The measured $n_e = 4 \times 10^{11}$ cm^{-3} for this data run gives the UHR-ECR separation as 3 cm. This involves a shift from 5.5 to 5.1 kG.

Figure 3-4 displays the x-ray signal at 50 μs versus B_t. The ECR layer for the 15.5 GHz microwaves would be 5.5 kG. The peak x-ray signal is at the ECR layer. The Hβ signals recorded at 100 and 200 μs peak at lower B_t values, the latter at about 5.1 kG. The shift of the Hβ peak relative to the x-ray peak is related to the transition from the ECR interaction to the UHR, as seen in the ISX-B movies of visible radiation.[3]

The radial I_s profiles migrate with increasing density (Figure 3-5). The shift of 4 cm of the 11.5 kW-I_s-rising edge is an indication of the shift of the interaction zone and is within the error of the B_t measurement. At roughly the same parameters, except for density, the 4.6 kW profile is peaked towards the ECR layer. The separation of the ECR and UHR regions at $n_e \sim 1 \times 10^{11}$ cm^{-3} is about 0.8 cm, which is less than the step size of the measurement. As anticipated, the radial migration of the I_s peak is density dependent.

The width of the I_s peak may be explained by the presence of the $\underline{E}_v \times \underline{B}_t$ drift. The plasma would be transported radially by that drift.

The T_e radial profile, as measured by a triple probe during the microwave pulse, has a uniform 50 eV value from the UHR layer across the tokamak channel (Figure 3-6). The triple probe may overestimate the bulk T_e due to a non-Maxwellian electron distribution. The 10 eV value of T_e, during the microwave pulse,

Figure 3-4. X-rays and Hβ profiles versus toroidal field. The x-ray peak (x) occurs at 5.6 kG early in time, 50 μs. For the 15.5 GHz pulse, this magnetic field is the ECR location. The Hβ peaks at 100 μs (Δ) and 200 μs (•) are to the low field side of the ECR and correspond to power absorption at the UHR. The microwave pulse was 300 μs long.

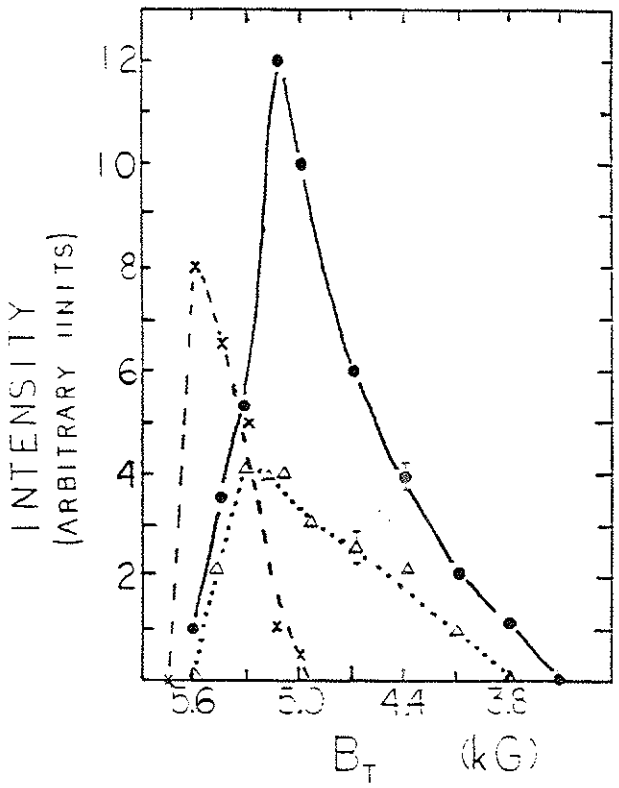

Figure 3-5. Radial ion saturation current profiles. The 4.6 kW (x) plasma at 600 μs is only slightly to the low field side of the ECR (~ -9 cm). The 11.5 kW density peak at 200 μs (Δ) is further to the low field side but represents higher density. The still higher density of the 11.5 kW case at 600 μs (o) is even further out radially. This corresponds to the migration of the interaction region to the UHR as the density rises. The higher the density the further the ECR-UHR separation. The microwave pulses were 600 μs long.

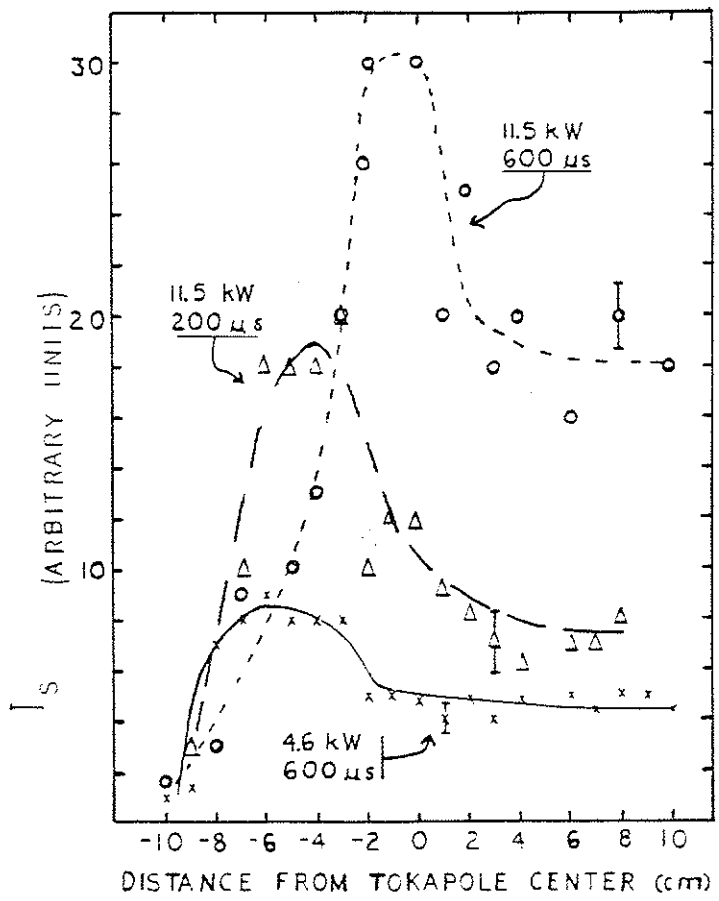

Figure 3-6. Triple probe T_e profiles with the resonance zone at -7 cm. The 15.5 GHz pulse lasted 500 μs. $T_e(r)$, with 4.6 kW of power, is shown for 400 μs (Δ) and 700 μs (x). An 11.5 kW pulse gives a similar triple probe T_e at 400 μs (Δ).